ACS NANO

www.acsnano.org

ARTICLE

从塑料废料中提取闪蒸石墨烯
Flash Graphene from Plastic Waste

Wala A. Algozeeb, Paul E. Savas, Duy Xuan Luong, Weiyin Chen, Carter Kittrell, Mahesh Bhat, Rouzbeh Shahsavari, and James M. Tour*

Cite This: *ACS Nano* 2020, 14, 15595−15604

Read Online

ACCESS | Metrics & More | Article Recommendations | Supporting Information

在这项工作中，提出了一种回收塑料废物产品的方法。
ABSTRACT: In this work, an approach to upcycling plastic waste (PW) products is presented. 该方法依靠闪蒸焦耳加热(FJH)将PW The method relies on flash Joule heating (FJH) 转化为闪蒸石墨烯(FG)。 to convert PW into flash graphene (FG). In addition to FG, the process results in the formation of carbon oligomers, hydrogen, and light hydrocarbons. 除FG外，该过程还会形成碳低聚物、氢和轻烃。 In order to make high-quality graphene, a sequential alternating current (AC) and direct current (DC) flash is used. 为了制备高质量的石墨烯，使用了顺序交流(AC)和直流(DC)闪蒸。 The FJH process requires no catalyst and works for PW mixtures, which makes the process suitable for handling landfill PW. FJH工艺不需要催化剂，适用于PW混合物，因此该工艺适用于处理垃圾填埋PW。 The energy required to convert PW to FG is ∼23 kJ/g or ∼$125 in electricity per ton of PW, potentially making this process economically attractive for scale-up. 将PW转化为FG所需的能量为23 kJ/g或每吨PW 125美元，这可能使该工艺在经济上具有扩大规模的吸引力。 The FG was characterized by Raman spectroscopy and had an I_{2D}/I_G peak ratio up to 6 with a low-intensity D band. 通过拉曼光谱对FG进行了表征，其I2D/IG峰比高达6，具有低强度D带。 Moreover, transmission electron microscopy and X-ray diffraction analysis show that the FG is turbostratic with an interlayer spacing of 3.45 Å. 此外，透射电子显微镜和X射线衍射分析表明，FG为涡轮层结构，层间间距为3.45。 The large interlayer spacing will facilitate its dispersion in liquids and composites. 较大的层间距将有助于其在液体和复合材料中的分散。 Analysis of FG dispersions in 1% Pluronic aqueous solution shows that concentrations up to 1.2 mg/mL can be achieved. FG在1%Pluronic水溶液中的分散分析表明，可以达到1.2 mg/mL的浓度。 The carbon oligomers that distilled from the process were characterized by Fourier transform infrared spectroscopy and have chemical structures similar to the starting PW. 通过傅立叶变换红外光谱对从该过程中蒸馏出的碳低聚物进行了表征，其化学结构类似于起始PW。 Initial analysis of gas-phase products shows the formation of considerable amounts of hydrogen along with other light hydrocarbons. 气相产物的初步分析表明，大量氢和其他轻烃一起形成。 As graphene is naturally occurring and shows a low toxicity profile, this could be an environmentally beneficial method to upcycle PW. 由于石墨烯是天然存在的，并且毒性较低，因此这可能是一种对PW进行升级循环的环境有益方法。

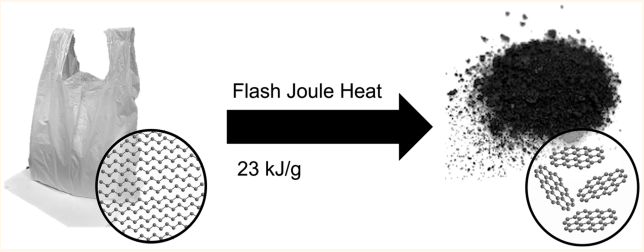

关键词：塑料废料、微塑料、回收、上循环、石墨烯、复合材料
KEYWORDS: *plastic waste, microplastics, recycling, upcycling, graphene, composites*

塑料废弃物污染已成为21世纪最紧迫的环境问题之一。
Plastic waste (PW) pollution is becoming one of the most pressing environmental concerns in the 21st century. 大量PW最终进入垃圾填埋场和海洋，导致形成微塑料和纳米塑料， A large fraction of PW ends up in landfills and the ocean, leading to the formation of micro- and nanoplastics 威胁海洋生物、微生物、有用细菌、和人类。 that threaten marine life,[2] microorganisms,[3,4] useful bacteria,[3] and humans.[5,6] 此外，石油化工产品的塑料生产具有高碳足迹。 In addition, plastics production from petrochemicals has a high carbon footprint. 必须对原油进行提取、蒸馏、精炼和净化，以形成石化原料，然后在排放大量温室气体的复杂能源密集型设施中进一步加工以生产塑料。 Crude oil must be extracted, distilled, refined, and purified to form petrochemical feedstocks that are further processed to produce plastic in complex and energy-intensive facilities that emit a large amount of greenhouse gases. 在塑料成型过程中以及运输给客户时，会排放额外的温室气体。 Additional greenhouse gases are emitted during the shaping of plastic for use and when transporting to customers. 在这种强烈的碳足迹过程之后，大多数合成塑料在倾倒到过度应力的垃圾填埋场或终止于海洋的水道之前只使用一次。 After this intense carbon footprint process, most of the synthesized plastic is used only once before dumping into overstressed landfills or waterways that terminate in oceans. 因此，将PW升级为更高价值的材料和化学品具有环境和经济优势。 Thus, upcycling PW to higher value materials and chemicals is environmentally and economically advantageous.

为了减少PW的数量，人们将大量精力投入到物理回收方面，即对塑料进行多次洗涤剂清洗，并对其进行再利用。 To reduce the amount of PW, much effort has been directed toward physical recycling, in which the plastic is detergent-washed multiple times and reshaped for reuse. 然而，物理回收有主要缺点，包括需要在研磨、研磨和杀菌之前对塑料进行人力密集型分类。 However, physical recycling has major drawbacks including the need for human-labor-intensive sorting of plastics prior to milling, grinding, and sterilizing. 处理PW的另一个途径是化学循环，即PW在惰性气氛中热解，有时在催化剂存在下，将塑料分解成更小的分子和油。 Another route for PW handling is chemical recycling, where PW is pyrolyzed in an inert atmosphere, sometimes in the presence of a catalyst, decomposing the plastic into smaller molecules and oils.[12,15] 此外，PW热解涉及将大型反应器加热至500-600 °C，消耗大量能源，同时使化学形成成本高昂，碳足迹大。 Moreover, PW pyrolysis involves heating large reactors up to 500−600 °C,[15] consuming sizable amounts of energy while making chemical formation expensive with a large carbon footprint. 化学回收的另一个缺点是，由于PW中存在添加剂和增塑剂等污染物，在热解过程中催化剂中毒。 Another drawback of chemical recycling is the poisoning of the catalyst during the pyrolysis process due to the presence of contaminants in PW, such as additives and plasticizer. 因此，在化学循环之前，必须对PW进行预处理以提取无机添加剂，以避免催化剂中毒。 For this reason, PW must be pretreated to extract inorganic additives prior to chemical recycling to avoid catalyst poisoning. 到目前为止，大多数报道的回收技术都不符合成本效益，因此只有9%的生产塑料被回收。 To date, most reported recycling technologies are not cost-effective, and thus only 9% of all produced plastic has been recycled.[16] 因此，寻求更绿色的回收或升级技术，后者发生在产品达到高于起始塑料的价值时。 Therefore, greener recycling or upcycling technologies are sought, with the latter occurring when the products attain a higher value than the starting plastic.

Received: July 28, 2020
Accepted: October 22, 2020
Published: October 29, 2020

https://dx.doi.org/10.1021/acsnano.0c06328
ACS Nano 2020, 14, 15595−15604

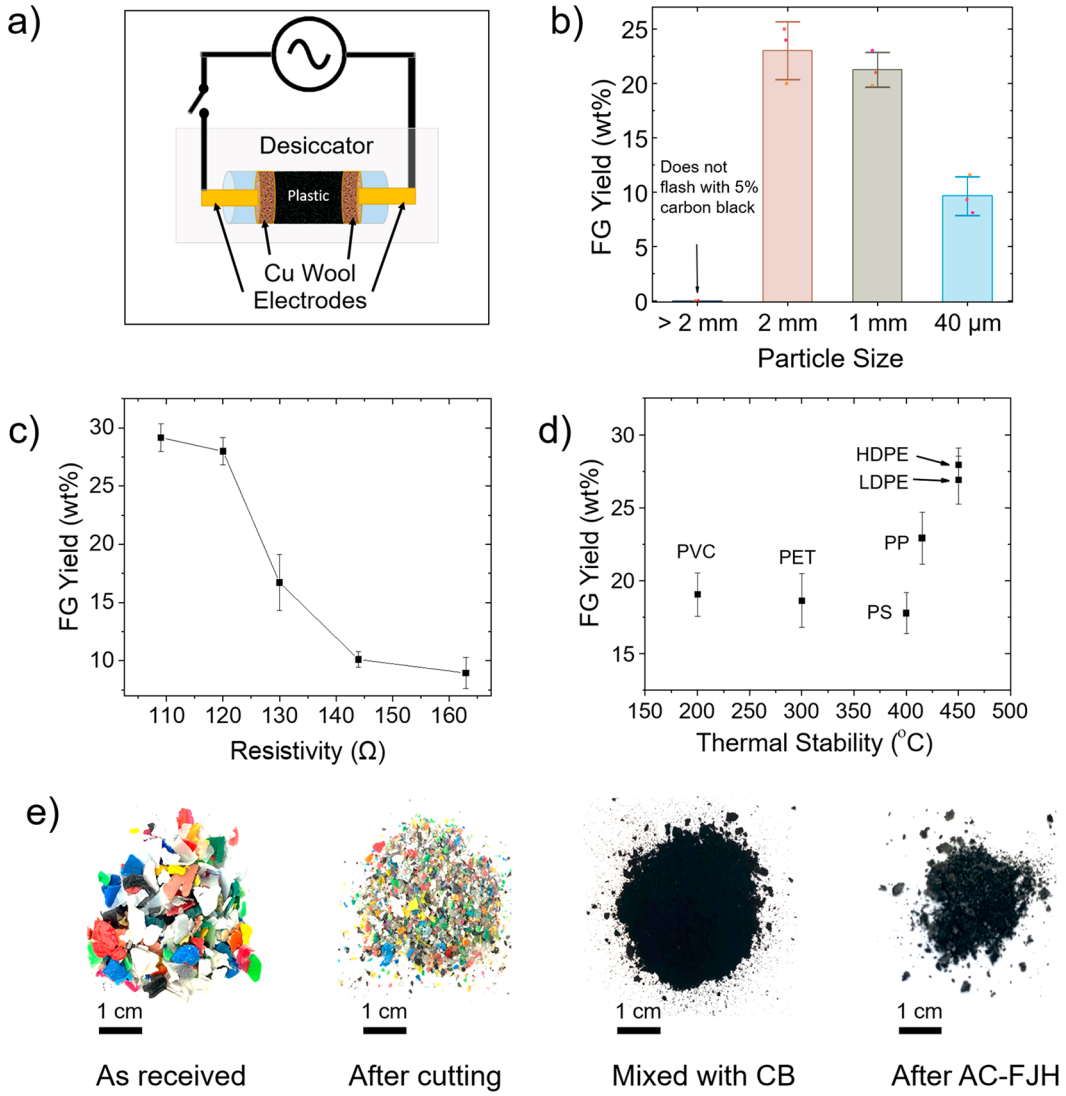

图1。(a)120 V交流电路示意图。(b)AC-FG从粒径为2 mm、1 mm和40 m、炭黑含量为5 wt%的HDPE中获得，初始电阻率为125。粒径>2 mm的样品没有闪蒸5%炭黑。误差条是三次样本运行的标准偏差。(c)HDPE/CB混合物的初始电阻率对AC-FG产率的影响。通过在两个电极之间施加更大的压缩(螺旋钳)，电阻率降低。图上的误差线是三次样本运行的标准偏差。(d)当初始电阻为120时，典型的AC-FG从不同的塑料中产生。误差条是三次样本运行的标准偏差。(e)从回收商处收到的消费后塑料照片(从左到右)；使用商用切割机切割后；与5 wt%炭黑混合后；并使用AC-FJH进一步转换为FG。

Figure 1. (a) Schematic of the 120 V AC circuit. (b) AC-FG yield from HDPE with 2 mm, 1 mm, and 40 μm particle size with 5 wt % CB at an initial resistivity of 125 Ω. Samples of particle size >2 mm did not flash with 5% CB. The error bars are standard deviation over three sample runs. (c) Effect of initial resistivity of the HDPE/CB mixture on AC-FG yield. The resistivity is lowered through the application of increased compression (screw vice) between the two electrodes. The error bars on the graph are standard deviation over three sample runs. (d) Typical AC-FG yields from different plastics when the initial resistance is 120 Ω. The error bars are standard deviation over three sample runs. (e) Pictures of (left to right) postconsumer plastic as received from a recycler; after cutting using a commercial cutter; after mixing with 5 wt % CB; and further conversion to FG using AC-FJH.

这项工作描述了处理PW时化学和物理回收的替代方法，它基于我们最近开发的直流(DC)闪蒸焦耳加热(DC-FJH)方法(图S1)，将碳源转换为石墨烯。该过程形成所谓的闪蒸石墨烯。

This work describes an alternative approach to chemical and physical recycling when dealing with PW, and it is based upon our recently developed direct current (DC) flash Joule heating (DC-FJH) method (Figure S1) to convert carbon sources into graphene, with the process forming what is called flash graphene. 该技术依靠电力在PW中诱导FJH。The technology relies on electricity to induce FJH in PW. 这会在短时间内将碳源推向高温。This drives the carbon source to high temperatures in a short time period. 这里的工作表明，在处理PW时，交流闪蒸焦耳加热(AC-FJH)(图S2)优于直流闪蒸焦耳加热，因为在这种情况下，它可以持续数秒，即8秒。The work here shows that alternating current (AC) flash Joule heating (AC-FJH) (Figure S2) is advantageous over DC-FJH when dealing with PW because it can be sustained for seconds, 8 s in this case. 这允许释放必要的挥发物，产生中间AC闪蒸石墨烯(AC-FG)，当通过拉曼光谱进行表征时，其I2D/IG峰值比在1.2和0.5之间，并且具有高强度D带。This permits the release of the necessary volatiles, producing an intermediate AC flash graphene (AC-FG) with a I_{2D}/I_G peak ratio between 1.2 and 0.5 and a high-intensity D band when characterized by Raman spectroscopy. 该工艺克服了在熔炉中对塑料进行热解的需要，在该过程中会损失大量能量。This process overcomes the need to pyrolyze the plastic in furnaces, where much of the energy is lost in the process. 然后，在单个DC-FJH脉冲上。Then, upon a single DC-FJH pulse, the intermediate AC-FG 当通过拉曼光谱进行表征时，中间AC-FG转化为I2D/IG峰值比在1到6之间和低强度D带的高质量涡轮层FG(tFG)。is converted to very high-quality turbostratic FG (tFG) with an I_{2D}/I_G peak ratio between 1 and 6 and low-intensity D band when characterized by Raman spectroscopy. 这种顺序交流和直流(ACDC)闪蒸工艺对于单流热塑性塑料和PW混合物的上循环是有效的。This sequential AC and DC (ACDC) flash process was shown to be effective for upcycling both single-stream thermoplastics and PW mixtures. 鉴于石墨烯对典型微生物、化学降解、和热降解的高稳定性，该技术提供了一种将PW转化为具有低毒性的稳定天然碳形式的方法。Given the high stability of graphene to typical microbial,[20,21] chemical,[22] and thermal degradation,[23] this technology offers a method for converting PW into a stable and naturally occurring form of carbon that has low toxicity.[24,25] 石墨烯团聚体是天然矿物石墨。Agglomerates of graphene are the natural mineral graphite.

结果和讨论 RESULTS AND DISCUSSION

使用商用研磨机研磨PW，并与5 wt%炭黑(CB)混合以获得导电混合物。PW was ground using a commercial grinder and mixed with 5 wt % carbon black (CB) to obtain a conductive mixture. The CB可以用之前运行的5 wt%FG替代。CB can be substituted with 5 wt % FG from a former run. The 塑料粉末被包装在一个石英管中，位于两个plastic powder was packed in a quartz tube between two

https://dx.doi.org/10.1021/acsnano.0c06328
ACS Nano 2020, 14, 15595−15604

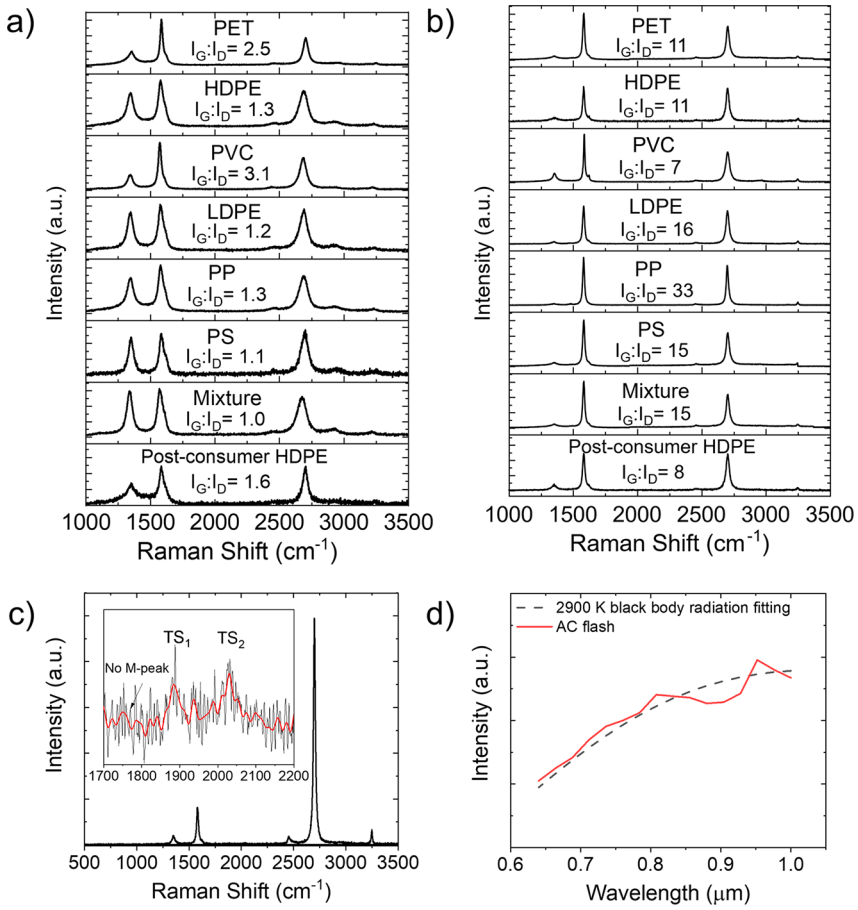

图2:(a)AC-FG和(b)ACDC-tFG的特征拉曼光谱。塑料混合物为40%HDPE、20%PP、20%PET、10%LDPE、8%PS和2%PVC。(c)从PVC中观察到的ACDC tFG的高涡轮层FG的拉曼光谱，显示扩展光谱中的涡轮层FG带。(d)使用红外光谱仪和黑体辐射拟合收集的AC-FJH过程的温度分布。

Figure 2. Characteristic Raman spectra of (a) AC-FG and (b) ACDC-tFG. Plastic mixture is 40% HDPE, 20% PP, 20% PET, 10% LDPE, 8% PS, and 2% PVC. (c) Raman spectrum of highly turbostratic FG observed for ACDC-tFG from PVC, showing the turbostratic FG bands in the expanded spectrum. (d) Temperature profile of the AC-FJH processes collected using an IR spectrometer and blackbody radiation fitting.

铜电极，并用AC-FJH(120 V，60 Hz)处理8s。AC-FJH电路的轮廓如图1a所示。AC-FJH设备的图片和电气示意图如图S2所示。在AC-FJH过程中，导电PW样品释放碳低聚物和挥发物，而FG在铜电极之间形成。

copper electrodes and was treated with AC-FJH (120 V, 60 Hz) for 8 s. An outline of the AC-FJH circuit is shown in Figure 1a. Pictures and electrical schematic of the AC-FJH equipment are in Figure S2. During the AC-FJH, the conductive PW sample releases carbon oligomers and volatiles, while FG is formed between the copper electrodes. The电极也可以由石墨或其他导电耐火材料制成。electrodes can also be made from graphite or other conductive refractory materials. There is ~0.5 mm of space between the电极和石英侧壁之间有0.5 mm的空间，允许挥发物从石英管中逸出。electrodes and the quartz sidewall, allowing for the volatiles to escape from the quartz tube. 为了安全起见，所有闪蒸程序必须在疏散的密闭室内进行(见支持信息中的安全说明)。All flashing procedures must take place inside an evacuated closed chamber for safety (see safety notes in the Supporting Information). 从AC-FJH过程中获得的FG称为AC-FG。FG obtained from the AC-FJH process is termed AC-FG. 使用不同粒径的塑料粉末发现，当使用5%炭黑时，粒径在1到2 mm之间的粉末可以获得最高的AC-FG产率。Plastic powders with different particle sizes were used to find that a powder with grain size between 1 and 2 mm gives the highest yield of AC-FG when 5% CB is used. 粒径大于2 mm的塑料粉末在与5 wt%炭黑混合时导电性不足以反应，而粒径小于50 μm的粉末在FJH过程中往往会从石英管及其松散配合的电极中逸出，导致AC-FG的产率大幅下降。Plastic powders with a grain size larger than 2 mm are not conductive enough to react when mixed with 5 wt % CB, whereas powders with a grain size smaller than 50 μm tend to escape from the quartz tube, with its loose fitting electrodes, during the FJH process, causing a large drop in the yield of AC-FG. 图1b显示了当2 mm、1 mm和40 μm高密度聚乙烯(HDPE)粉末颗粒分别经受AC-FJH以分别获得23%、21%和10%的AC-FG产率时，AC-FG的产率。Figure 1b shows the yield of AC-FG when 2 mm, 1 mm, and 40 μm particles of high-density polyethylene (HDPE) powders were separately subjected to AC-FJH to obtain 23, 21, and 10% AC-FG yield, respectively. 另一个对AC-FG产量起重要作用的因素是样品的初始电阻率；将塑料粉末压缩到石英管中会降低初始电阻率增加，FG产量增加。Another factor that plays an important role in the yield of AC-FG is the initial resistivity across the sample; compressing the plastic powders into the quartz tube lowers the initial resistivity and increases the FG yield. 图1c显示了从两个电极之间不同样品压缩得出的不同初始电阻率下闪蒸HDPE粉末获得的AC-FG的产率。Figure 1c shows the yield of AC-FG obtained from flashing HDPE powder at different initial resistivity derived from different sample compressions between the two electrodes. AC-FJH可用于从不同热塑性塑料中生产FG，包括聚对苯二甲酸乙二醇酯(PET)、HDPE、聚氯乙烯(PVC)、低密度聚乙烯(LDPE)、聚丙烯(PP)和聚苯乙烯(PS)；FG产量因母体材料而异。AC-FJH was found to be useful for FG production from different thermoplastics including polyethylene terephthalate (PET), HDPE, poly(vinyl chloride) (PVC), low density polyethylene (LDPE), polypropylene (PP), and polystyrene (PS); the FG yield varied based on the parent material. 如图1d所示，发现从不同热塑性塑料中获得的AC-FG的产率与母体材料的热稳定性相关；塑料的热稳定性越高，FG产率越高，生成的挥发性低聚物越少。As shown in Figure 1d, the yield of AC-FG obtained from different thermoplastics was found to correlate to the thermal stability of the parent material; the higher the thermal stability of the plastic, the higher the FG yield and the less volatile oligomers generated. 注意，产率是根据聚合物的碳含量计算的。Note that the yields were calculated based on the carbon content of the polymer. 添加的CB在FJH时转化为FG，对总产量的贡献小于4%。Added CB converts to FG upon FJH, contributing <4% to the total yield. 图1e显示了来自商业回收商(德克萨斯州杰克逊维尔Polywize)的消费后高密度聚乙烯塑料的大块碎片，然后使用商业切割机切割，与5 wt%炭黑混合，最后在FJH后转换为AC-FG。Figure 1e shows large shreds of postconsumer HDPE plastic from a commercial recycler (Polywize, Jacksonville, TX), which was then cut using a commercial cutter, mixed with 5 wt % CB, and finally, after FJH, converted into AC-FG. 与塑料热解过程不同，不需要高温炉或催化剂。Unlike plastic pyrolysis processes, there is no need for a high-temperature furnace or catalyst. The AC-FJH工艺产生中间FG，通过短DC-FJH脉冲将其转换为高质量FG(见下文)。AC-FJH process produces an intermediate FG, which is transformed into high-quality FG by a short DC-FJH pulse (see below). 我们试图用5%炭黑闪蒸二氧化硅(SiO_2)，但混合物的导电性不足以闪蒸。We tried to flash silica (SiO_2) with 5% CB, but the mixture was not conductive enough to flash. 在添加25%炭黑后，该材料的导电性足以闪蒸，但没有产生石墨烯。After 25% CB was added, the material was conductive enough to flash but did

https://dx.doi.org/10.1021/acsnano.0c06328
ACS Nano 2020, 14, 15595−15604

表1。从拉曼光谱分析2D、G和D带

Table 1. Analysis of the 2D, G, and D Bands from the Raman Spectra

	2D				G				D			
	AC-FG		ACDC-tFG		AC-FG		ACDC-tFG		AC-FG		ACDC-tFG	
plastic type	position (cm^{-1})	fwhm (cm^{-1})	position (cm^{-1})	fwhm (cm^{-1})	position (cm^{-1})	fwhm (cm^{-1})	position (cm^{-1})	fwhm (cm^{-1})	position (cm^{-1})	fwhm (cm^{-1})	position (cm^{-1})	fwhm (cm^{-1})
PET	2682	63	2701	31	1573	32	1581	18	1342	55	1352	62
HDPE	2686	82	2701	28	1581	53	1581	18	1343	75	1350	35
PVC	2682	64	2700	36	1573	32	1586	13	1342	55	1354	43
LDPE	2686	76	2701	28	1581	52	1581	18	1343	58	1350	35
PP	2686	81	2699	20	1581	53	1581	16	1343	74	1350	60
PS	2694	70	2701	18	1581	46	1582	18	1349	45	1352	62
average	2689	71	2701	27	1580	44	1582	17	1345	67	1351	50
STDV	7	13	1	7	4	11	2	2	4	17	2	13

因此，与高达25%炭黑混合的二氧化硅不会产生石墨烯。

not yield graphene. Thus, silica mixed with up to 25% CB does not produce graphene.

使用拉曼光谱测定FG的质量。

The quality of FG was determined using Raman spectroscopy. AC-FJH was found to result in the formation of FG with different I_{2D}/I_G peak ratios, as well as different D band intensities. Figure 2a displays the mean characteristic Raman spectrum of FG obtained from the AC-FJH pretreatment process, showing broad 2D and G bands and substantial D bands. The quality of AC-FG was significantly upgraded using a single 500 ms DC pulse (see Figure S1 for DC circuit outline) to obtain high-quality turbostratic FG (tFG) from many kinds of plastic (Figure 2b). tFG obtained from AC-FJH followed by DC-FJH is termed ACDC-tFG. Detailed analysis (Lorentzian fitting) was performed on each of the collected Raman spectra; fitting data may be found in the Figures S3−S14. The collected Raman spectra for both AC-FG and ACDC-tFG have excellent Lorentzian fitting with $R^2 \geq 0.98$, indicating the absence of Bernal stacking. When characterizing tFG, the I_G/I_D peak ratio is an important indicator of the degree of disorder and the quality of tFG. A higher I_G/I_D peak ratio is indicative of a lower degree of disorder and higher tFG quality. Figure 2a,b show that the I_G/I_D peak ratio increases significantly in ACDC-tFG when compared to AC-FG. This suggests that the DC-FJH of AC-FG reduce disorder and result in the formation of high-quality tFG. The formation of the low D band could also be indicative of the formation of large sheets with low edge densities and low disorder or from the formation of zigzag edges that reduce the intensity of the D band. Table 1 lists the position and the full width at half-maxima (fwhm) of the 2D, G, and D bands of AC-FG and ACDC-tFG. DC-FJH transforms the quality of AC-FG to obtain sharp 2D and G bands and low D band intensity when characterized by Raman spectroscopy. Upon DC-FJH, the 2D band shifts from 2689 to 2700 cm^{-1}, and the fwhm decreases from 71 to 27 cm^{-1}, resulting in a sharp 2D band that matches the data reported for high-quality turbostratic graphene.[19,31−33] The G band shifts from 1580 to 1584 cm^{-1}, and the fwhm decreases from 44 to 16 cm^{-1}, giving a sharp G band. Unlike typically furnace-grown graphene, the I_{2D}/I_G peak ratio is not a good indicator of the quality of tFG. The I_{2D}/I_G peak height ratio is mainly an indicator of the number of turbostratic layers[34] (see Supporting Information for more information about assessing the quality of tFG).

图2a显示了从AC-FJH预处理过程中获得的FG的平均特征拉曼光谱，显示了广泛的2D和G带以及大量的D带。

使用单个500毫秒直流脉冲(直流电路轮廓见图S1)显著提升了交流FG的质量，以从多种塑料中获得高质量涡轮层流FG(tFG)(图2b)。

从AC-FJH和DC-FJH获得的tFG称为ACDC tFG。

对收集的每个拉曼光谱进行详细分析(洛伦兹拟合)；拟合数据可在图S3和S14中找到。

收集到的AC-FG和ACDC-tFG的拉曼光谱具有良好的洛伦兹拟合，R²为0.98，表明没有伯纳尔堆叠。

当表征tFG时，IG/ID峰值比是tFG紊乱程度和质量的重要指标。

IG/ID比值越高，表明紊乱程度越低，tFG质量越高。

图2a,b表明，与交流-FG相比，交流直流输电线路图中的IG/ID峰值比显著增加。

这表明AC-FG的DC-FJH减少了无序并导致高质量tFG的形成。

低D带的形成也可能表明形成了边缘密度低、无序度低的大板，或形成了降低D带强度的锯齿形边缘。

表1列出了AC-FG和ACDC-tFG的2D、G和D带的半最大值(FWHM)位置和全宽。

当通过拉曼光谱进行表征时，DC-FJH转换AC-FG的质量，以获得清晰的2D和G带以及较低的D带强度。

在DC-FJH时，2D带从2689cm-1移动到2700cm-1，半高宽从71cm-1减少到27cm-1，从而产生一个尖锐的2D带，与高质量涡轮层石墨烯的报告数据相匹配。

G带从1580cm-1移动到1584cm-，半高宽从44cm-1减少到16cm-1，产生一个尖锐的G带。

与典型的炉生长石墨烯不同，I2D/IG峰比值不是tFG质量的良好指标。

I2D/IG峰高比主要是涡轮层数量的指标34(有关评估tFG质量的更多信息，请参阅支持信息)。

High-quality FG is difficult to obtain by direct DC-FJH treatment of PW without the AC-FJH. AC-FJH is essential for removing more volatiles from the PW to obtain high-quality FG (see Figures S15 and S16 for Raman spectra and thermogravimetric analysis (TGA) of FG obtained when only DC-FJH was used to make FG from plastics). Figure 2c shows the Raman spectrum of ACDC-tFG from PVC with I_{2D}/I_G peak ratio equal to 6, in which the TS_1 and TS_2 bands are observed that are indicative of the pure turbostratic morphology of tFG. Previous studies show that turbostratic graphene with some Bernal stacked layers would have a large M-peak that is not observed in our FG. During the AC-FJH processes, the temperature rises to ∼2900 K, forcing the C−C bonds to break and rearrange to the more stable graphene. Most excess energy is released via light radiation, which results in rapid cooling of the carbon material and a bright flash with every discharge. The fast cooling rate leads to the random arrangement of the graphene sheets to obtain tFG. There is insufficient time to form AB-stacked layers. When the cooling rate was slowed by trapping the IR and UV emissions inside the flashing tube, graphene with a broad 2D peak (fwhm of 65 cm^{-1}) and was observed. The peaks did not show good Lorentzian fitting, indicating the formation of AB-stacked graphene upon slowing the cooling rate (Figure S17). The same phenomena is observed with long DC-FJH pulse durations; longer heating times induce the formation of AB-stacked graphene. Figure 2d shows the temperature profile of the AC-FJH processes collected *via* an in-house-built infrared (IR) spectrometer (spectrometer components are shown in Figure S18). The collected data were fitted with blackbody radiation curves to find that the temperature increases to 2900 K during the AC-FJH process. The DC-FJH flash is known to reach ∼3100 K, which is the temperature required to obtain high-quality graphene, as shown in previous work. Recordings of the current passing through the sample during the DC-FJH process shows that 180 A of electricity passes through the sample in ∼100 ms discharge time (Figure S19). FJH to such high temperatures volatilizes non-carbon elements, leaving a highly pure form of graphene. Note that most elements, including metals and silicon, sublime below 2900 K, whereas carbon sublimes at ∼3900 K. This purification mechanism obviates the need to remove contaminates, such as plasticizers, residual food, and even clays, before using FJH to obtain high-quality FG. For example, PET carbonated beverage bottles contain ∼10% nanoclay that is added as a gas barrier.[38] These nanoclays sublime (possibly after reduction) from the PW matrix during the FJH process to produce FG (see Figure S20 for TGA of PET before and after FJH). FJH was shown to be effective for converting PW mixtures to FG, which makes this process a good choice for eliminating the labor-intensive sorting steps necessitated by other recycling/reuse processes.

只有DC-FJH用于从塑料中制备FG)。

图2c显示了I2D/IG峰比等于6的PVC中ACDC tFG的拉曼光谱，其中观察到TS1和TS2带，表明tFG的纯涡轮层形态。

之前的研究表明，具有一些伯纳尔堆叠层的涡轮层石墨烯将具有在我们的FG中未观察到的大M峰。

在AC-FJH过程中，温度上升到2900 K，迫使C-C键断裂并重新排列为更稳定的石墨烯。

大多数多余的能量是通过光辐射释放的，这会导致碳材料迅速冷却，每次放电都会发出明亮的闪蒸。

快速冷却速度导致石墨烯片的随机排列以获得tFG。

没有足够的时间形成AB堆叠层。

当通过在闪蒸管内捕获红外和紫外线发射来减缓冷却速度时，石墨烯具有宽的2D峰值(半高宽为65cm1)

并进行了观察。

这些峰没有表现出良好的洛伦兹拟合，表明在减慢冷却速度时形成AB堆叠石墨烯(图S17)。

同样的现象在长的DC-FJH脉冲持续时间中观察到；较长的加热时间会导致AB堆叠石墨烯的形成。

图2d显示了通过内置红外光谱仪收集的AC-FJH过程的温度分布(光谱仪组件如图S18所示)。

收集的数据与黑体辐射曲线拟合，发现在AC-FJH过程中温度上升到2900 K。

众所周知，DC-FJH闪蒸达到3100 K，这是获得高质量石墨烯所需的温度，如之前的工作所示。

直流-FJH过程中通过样品的电流记录表明，在100毫秒的放电时间内，180 A的电流通过样品(图S19)。

FJH在如此高的温度下挥发非碳元素，留下高纯度的石墨烯。

注意，大多数元素，包括金属和硅，在2900 K以下升华，而碳在3900 K下升华。[36]

在使用FJH获得高质量FG之前，这种净化机制无需去除污染物，例如增塑剂、残留食物，甚至粘土。

例如，PET碳酸饮料瓶含有10%的纳米粘土，作为气体屏障添加。

38将其进行AC-FJH处理，观察到纳米粘土在FJH过程中从PW基质升华(可能在还原后)以产生FG(关于FJH前后PET的TGA，见图S20)。

AC-FJH对于从PW中去除更多挥发物以获得高质量FG至关重要(在以下情况下获得的FG的拉曼光谱和热重分析(TGA)见图S15和S16)

FJH被证明是将PW混合物转化为FG的有效方法，这使得该工艺成为消除其他回收/再利用工艺所需的劳动密集型分拣步骤的良好选择。

https://dx.doi.org/10.1021/acsnano.0c06328
ACS Nano 2020, 14, 15595−15604

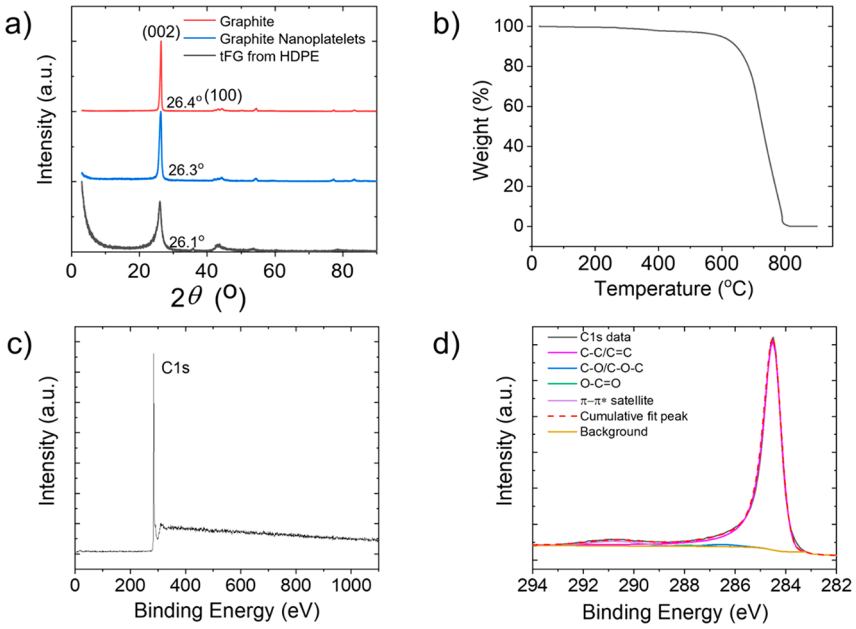

图3、(a) HDPE中ACDC tFG的XRD。(b) HDPE中ACDC-tFG的热重分析(空气，15 °C/min)和(C)HDPE中ACDC-tFG的XPS扫描调查。(d) HDPE中ACDC tFG的高分辨率C 1s XPS光谱。

Figure 3. (a) XRD of ACDC-tFG from HDPE. (b) TGA (air, 15 °C/min) of ACDC-tFG from HDPE and (c) survey XPS scan of ACDC-tFG from HDPE. (d) High-resolution C 1s XPS spectrum of ACDC-tFG from HDPE.

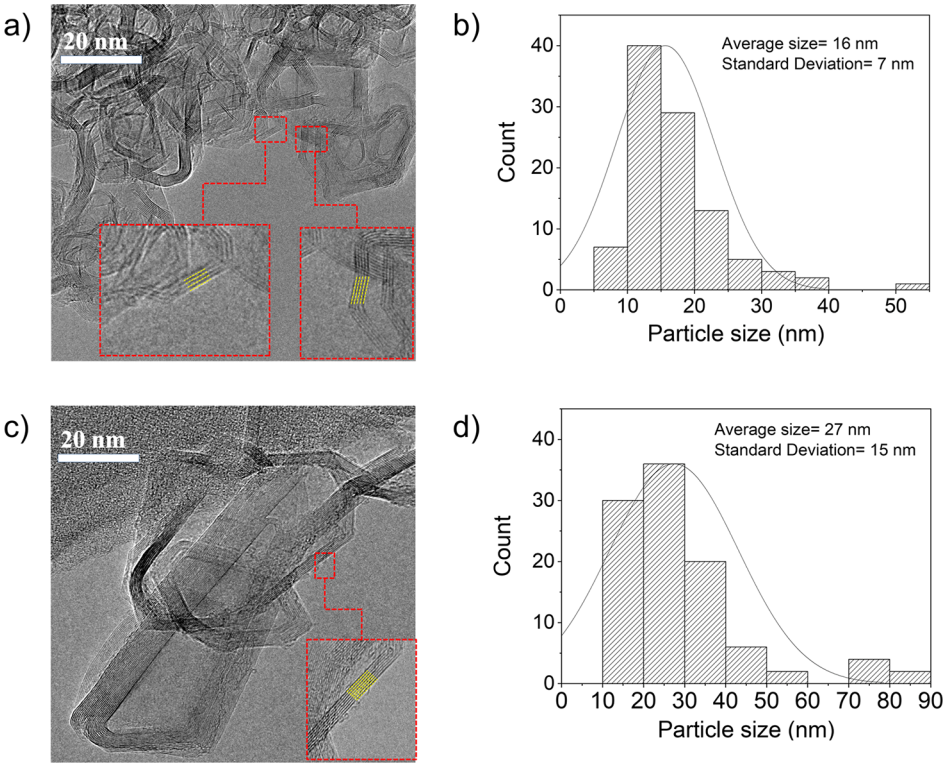

图4、(a) HDPE中AC-FG的TEM图像和(b)AC-FG的颗粒数(n=100)。(c) HDPE中ACDC-tFG的TEM图像和(d)HDPE中ACDC-tFG的颗粒

Figure 4. (a) TEM image of AC-FG from HDPE and (b) particle count of AC-FG (n = 100). (c) TEM image of ACDC-tFG from HDPE and (d) particle count of ACDC-tFG from HDPE (n = 100).

从不同PW产品中获得的ACDC tFG的X射线衍射(XRD)显示两个峰出现在26.1(002)和45°(001)(图S21显示了不同塑料的tFG的XRD)。

X-ray diffraction (XRD) of ACDC-tFG obtained from different PW products shows two peaks occurring at 26.1 (002) and 45° (001) (Figure S21 has XRD of tFG from different plastics). 与石墨和石墨纳米片(图3a)(两者均具有AB堆叠层)Compared to graphite and graphite nanoplatelets (Figure 3a), both of which have AB-stacked layers, ACDC-tFG has a (002) peak that occurs at a slightly lower 2θ with I_c = 3.45 Å, indicating larger interlayer distance between the ACDC-tFG sheets. ACDC-tFG的(002)峰值 The (002) peak of ACDC-tFG has a tail that extends to low 2θ, which is due to rotational disorder between the ACDC-tFG layers. 图3b显示了Figure 3b shows the TGA of ACDC-tFG from the HDPE with thermal decomposition commencing at ∼625 °C in air. HDPE中ACDC tFG的热重分析，在625 °C的温度下在空气中开始热分解。The high thermal stability is indicative of the high degree of crystallinity and low defects of the tFG structure, as defects often lower the thermal stability of graphene. 高热稳定性表明tFG结构的高结晶度和低缺陷，因为缺陷通常会降低石墨烯的热稳定性。HDPE中ACDC-tFG的X射线光电子能谱(XPS)A survey X-ray photoelectron spectroscopy (XPS) of ACDC-tFG from HDPE shows pure 研究表明

有一个延伸到低2的尾部，这是由于ACDC-tFG层之间的旋转无序造成的。

https://dx.doi.org/10.1021/acsnano.0c06328
ACS Nano 2020, 14, 15595−15604

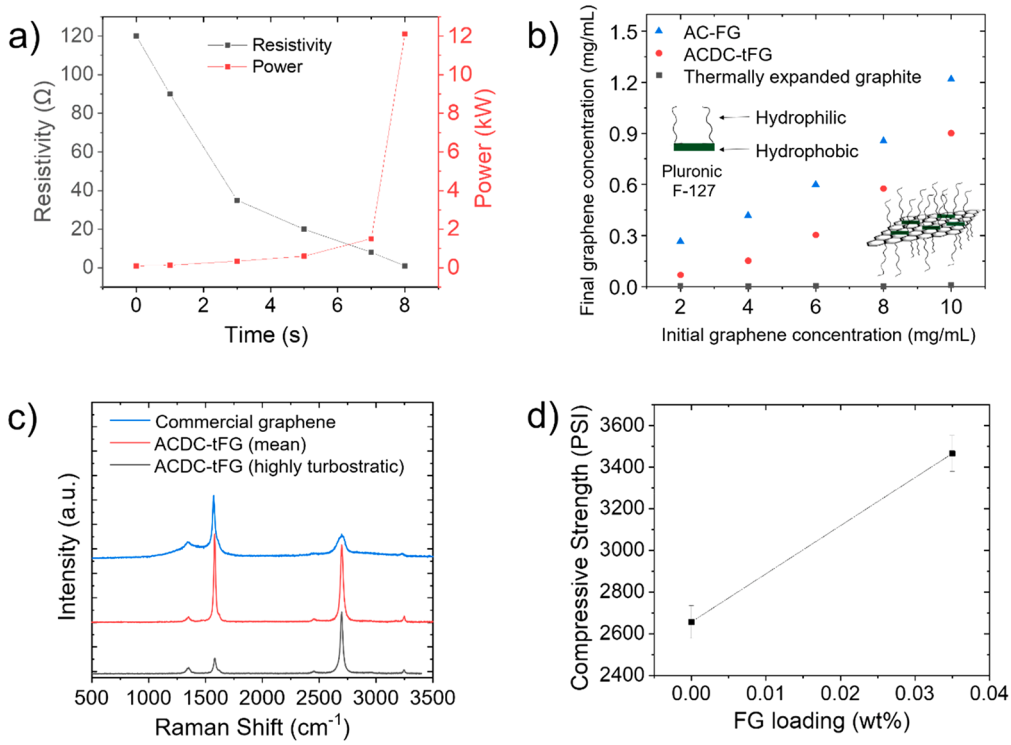

图5、(a) HDPE AC-FJH过程中的电阻率值和功耗。(b)在离心之前(初始)和之后(最终)，从HDPE和1%Pluronic中对热膨胀石墨、AC-FG和ACDC-tFG进行浴声处理分散浓度。(c) ACDC tFG(来自HDPE)和商用石墨烯的拉曼光谱。(d)抗压强度水泥/AC-FG复合材料(FG来自HDPE)。

Figure 5. (a) Resistivity values and power consumed during the AC-FJH process of HDPE. (b) Bath-sonicated dispersion concentration of thermally expanded graphite, AC-FG and ACDC-tFG from HDPE and in 1% Pluronic before (initial) and after (final) centrifugation. (c) Raman spectra of ACDC-tFG (from HDPE) and commercial graphene. (d) Compressive strength cement/AC-FG composites (FG from HDPE).

不存在可检测的杂原子的碳成分(图3c)。carbon composition without the detectable presence of heteroatoms (Figure 3c). 来自HDPE的ACDC-tFG的高分辨率碳XPS(图3d)High-resolution carbon XPS of ACDC-tFG from HDPE (Figure 3d) shows large C−C/C═C 显示在284.5 eV时出现较大的C/C峰。peaks occurring at 284.5 eV. 在286.5和288ev处分别观察到痕量co/co-C和O-co-XPS峰。Trace C−O/C−O-C and O−C═O O XPS peaks were observed at 286.5 and 288 eV, respectively. 注意，氯含量为50%的PVC在闪蒸时形成高纯度FG，通过高分辨率XPS检测不到氯的存在(图S22)。Note that PVC, which has ∼50% chlorine content, formed high-purity FG upon flashing, without a detectable presence of chlorine by high-resolution XPS (Figure S22). 这表明FJH方法对于处理难以重新利用的PW是有效的。This indicates that the FJH method is effective for handling PW that is otherwise difficult to repurpose. 当闪蒸PVC时，盐酸(HCl)预计会在AC-FJH过程中与其他碳氢化合物一起作为副产品释放。When flashing PVC, hydrochloric acid (HCl) is expected to be released during the AC-FJH process as one of byproducts along with other hydrocarbons. 与传统的化学回收类似，HCl可以使用石灰吸收器从其他废水中分离出来。Similar to conventional chemical recycling, HCl can separated from other effluents using a lime absorber.[9]

AC-FG的TEM图像显示了高度石墨化的薄片(图4a)，平均尺寸为16 nm(图4b)。A TEM image of AC-FG shows highly graphitic sheets (Figure 4a) with an average size of 16 nm (Figure 4b). AC-FG包括四个堆叠涡轮结构层的平均值(图S23)。AC-FG comprise an average of four stacked turbostraic layers (Figure S23). 从TEM图像中，发现AC-FG层之间的间距为3.45(图S24)。From the TEM images, the spacing between the AC-FG layers was found to be 3.45 Å (Figure S24). 图4c显示了平均薄片尺寸为27 nm的ACDC tFG的TEM图像(图4d)，其大于AC-FG。Figure 4c shows a TEM image of ACDC-tFG with an average sheet size of 27 nm (Figure 4d), which is larger than that of the AC-FG. 这表明，在AC-FJH工艺之后，DC-FJH促进了ACDC tFG板的横向生长。This suggests that following the AC-FJH process with DC-FJH promotes the lateral growth of the ACDC-tFG sheets. 由于D带的强度与表面到边缘的密度相关，因此DC-FJH后板材尺寸的增加与拉曼光谱中D带的减少一致；较小的石墨烯片通常具有较高的D带强度。The increase in sheet size upon DC-FJH agrees with the decrease in the D band in the Raman spectra because the intensity of the D band correlates to the surface to edges density; smaller graphene sheets often have higher D band intensities. 观察到DC-FJH导致堆叠FG板的数量增加。DC-FJH was observed to result in an increase in the number of stacked FG sheets. ACDC tFG的TEM图像显示，每页平均有六层tFG(图S25)，平均层间距为3.45。TEM images of ACDC-tFG show an average of six layers (Figure S25) of tFG per sheet with an average interlayer spacing of 3.45 Å. 根据TEM图像计算的层间距离如图S26所示。The interlayer distance calculations from the TEM images are included in Figure S26. 夹层TEM图像的距离与XRD和Raman数据一致，支持ACDC-tFG涡轮层形貌的结论。The interlayer distance from the TEM images agrees with the XRD and Raman data that support the conclusion of the turbostratic morphology of ACDC-tFG.

为了计算将混合PW转换为FG所需的能量，在FJH期间监测了样品的电阻率。To calculate the energy required to covert mixed PW to FG, the resistivity across the sample was monitored during the FJH. 观察到样品的电阻率随时间下降，如图5a所示。The resistivity across the sample was observed to drop with time, as shown in Figure 5a.

从1.0 g混合PW开始，含40%HDPE、20%PP、20%PET、10%LDPE、8%PS和2%PVC，其碳含量为81 wt%(剩余物为H、O和Cl)，混合PW形成0.18 g(22%产率)的中间AC-FG，剩余物为挥发性化合物；从石英管的侧壁上分离出一些蜡(见下文)。Starting from 1.0 g of mixed PW, with 40% HDPE, 20% PP, 20% PET, 10% LDPE, 8% PS, and 2% PVC, which is 81 wt % carbon content (the remainder being H, O, and Cl), the mixed PW forms 0.18 g (22% yield) of intermediate AC-FG with the remainder being volatilized compounds; some waxes were isolated from the sidewalls of the quartz tube (see below). 将0.18 g中间AC-FG转化为高质量ACDC-tFJH石墨烯几乎是定量的，因此，根据ACDC-FJH组合方案，从混合PW中获得的高质量tFG总收率为22%。The conversion of the 0.18 g of intermediate AC-FG into high-quality ACDC-tFJH graphene is nearly quantitative, hence there is a 22% overall yield of high-quality tFG from mixed PW 当我们从1.0 g HDPE而不是混合PW开始时，经过ACDC-FJH后，高质量tFG的产率为0.23 g(由于HDPE是重量86%的碳，因此产率为27%)。following the combination ACDC-FJH protocol. When we start with 1.0 g of HDPE instead of mixed PW, the yield is 0.23 g (27% yield since HDPE is wt 86% carbon) of high-quality tFG after ACDC-FJH. 我们假设，如果我们建造一个压力容器，能够在FJH步骤中保留更多的挥发性成分，以实现更高的整体转化率，那么石墨烯的产率可以显著提高。We presume that the yield of graphene can be substantially increased if we build a pressure vessel that can retain more of the volatile components during the FJH steps for higher overall conversion.

AC-FJH过程中消耗的能量为21 kJ/g。The energy consumed during the AC-FJH processes is ∼21 kJ/g. DC-FJH所需的能量为13 kJ/g，但我们的DC-FJH仅为原始1.0 g混合塑料的0.18 g。The energy required for the DC-FJH is ∼13 kJ/g, but we are only DC-FJH 0.18 g of the original 1.0 g of mixed plastic. 总的来说，需要23 kJ才能将1.0 g混合PW转化为0.18克优质tFG。In total, 23 kJ is required to convert 1.0 g of mixed PW into 0.18 g of high-quality tFG. 能量计算如图S27所示。The energy calculation is shown in Figure S27. 这意味着将1吨PW转化为180公斤高质量tFG加挥发物的电力成本为124美元。This translates to $124 in electricity cost to convert 1 ton of PW into 180 kg of high-quality tFG plus volatiles. 这使得使用该技术的塑料升级成本与传统技术相比具有竞争力This makes the cost of upcycling plastic using this technology competitive when compared to conventional

https://dx.doi.org/10.1021/acsnano.0c06328
ACS Nano 2020, 14, 15595−15604

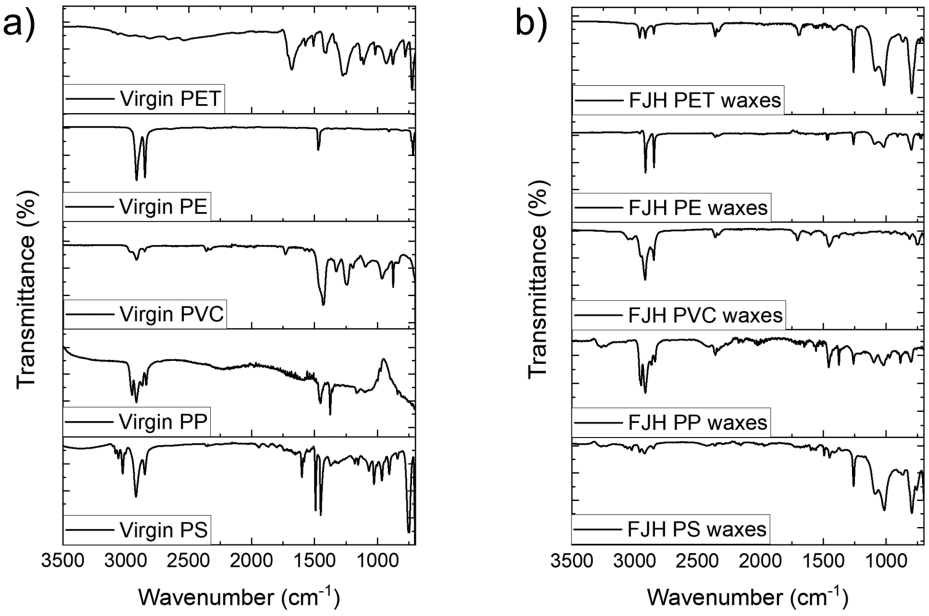

图6、(a) AC-FJH前后塑料和(b)蜡的红外光谱。
Figure 6. (a) IR spectra of the plastics before and (b) waxes after AC-FJH.

物理和化学回收技术。目前，回收技
physical and chemical recycling technologies. Currently,
术并不经济，这导致生产回收塑料的成本高于原始塑料。
recycling technologies are not economical, which results in
producing recycled plastic that is higher in cost than virgin
这反过来又导致对再生塑料的消费偏好高于再生塑料，增加了塑料污染和温室
plastic. This, in turn, leads to favoring the consumption of
气体排放(再生塑料和再生塑料的价格见表S1)。
virgin plastic over recycled plastic, increasing plastic pollution
and greenhouse gas emissions (see Table S1 for prices of
recycled and virgin plastics).
图5a揭示了tFG的形成机制。
Figure 5a gives insight into the mechanism of formation of
在AC-FJH中施加电压之前，我们先从高电阻率(低电导率)的AHD和CB混合物开始。
tFG. Prior to voltage application in the AC-FJH, we start with
a HDPE and CB mixture with high resistivity (low
在进行AC-FJH时，电流流经导电CB，产生大量热量，使非导电塑料碳
conductivity). As we proceed with AC-FJH, the current
化，导致电阻率随时间下降，在AC-FJH过程结束时形成富碳AC-FG。
flows *via* the conductive CB generating a large amount of heat
that carbonizes the nonconductive plastic, causing the
resistivity to drop with time, forming carbon-rich AC-FG by
此时，从图2a中收集的拉曼光谱可以明显
the end of the AC-FJH process. At this point, evident by the
看出，AC-FG未完全石墨化，并表现出相当多的无序，这表明AC-FJH过程中的大部分应用能
collected Raman spectra in Figure 2a, AC-FG is not fully
量通过去除挥发物而不是石墨化来应用于炭化塑料。
graphitized and exhibits a considerable amount of disorder,
indicating that most of the applied energy in the AC-FJH
process is applied toward carbonizing plastics by removing
在AC-FG的DC-FJH时，电流在AC-FG上
volatiles rather than graphitizing it. Upon DC-FJH of AC-FG,
均匀分布，产生热量，石墨化并修复AC-FG中存在的缺陷和无序，以在ACDC-FJH过程结束时
the current is uniform across the AC-FG, generating heat that
获得高质量的tFG。
graphitizes and heals the defects and disorder present in the
AC-FG to obtain high-quality tFG by the end of the ACDC-
FJH process.[19,35]
石墨烯的分散度是影响石墨烯在复合材料中加工性能的重要参数之一。
The degree of graphene dispersibility is one of the important
parameters that influences the processability of graphene into
Pluronic表面活性剂价格低廉，由于其亲水尾部和疏水核心，通常用于
composites. Pluronic surfactants are low in price and often
制备稳定的水性石墨烯分散体。
used to make stable aqueous graphene dispersions because of
their hydrophilic tails and hydrophobic cores.[42,43] The
研究了FG
在1%Pluronic F-127水溶液中的分散性，发现浓度高达
dispersibility of FG was studied in 1% aqueous Pluronic F-
127 solution to find that dispersions with concentrations up to
AC-FG可达到1.2 mg/mL，如图所示
1.2 mg/mL were attainable with AC-FG, as shown in Figure
ACDC-tFG分散体的浓度低于AC-FG，这可能是由于ACDC-tFG的薄片尺寸比AC-FG大。
5b. ACDC-tFG dispersions were lower in concentration than
that of AC-FG, which could be due to the larger sheet size of
然而，AC-FG和ACDC-tFG分散浓度均显著
ACDC-tFG compared to AC-FG. However, both AC-FG and
高于文献中报道的许多浓度。
ACDC-tFG dispersion concentrations are significantly higher
than many concentrations reported in the literature.[42,44] The
实现高
浓度FG分散的能力可能是由于涡轮层流的形态更容易实现
ability to achieve FG dispersions with high concentration is
likely due to the turbostratic morphology that makes is easier
克服FG层之间较弱的范德华相互作用。
to overcome weaker van der Waals interactions between the
当使用石墨时，只有当石墨烯和溶剂的净表面能大于AB堆叠层之间的强烈
FG layers. When working with graphite, exfoliation of the
范德华相互作用时，层才会发生剥落。
layers only occurs when the net surface energy of the graphene
and the solvent is greater than the strong van der Waals
interactions between the AB-stacked layers.[49] For this reason,
因此，石墨烯从石墨中
分散通常需要昂贵的有机溶剂和高超声功率，而tFG分散不需要这些。
graphene dispersion from graphite usually requires costly
organic solvents and high sonication power, which are not
required for tFG dispersions. Therefore, dispersions made
因此，由石墨制成的分散体的浓度远低于
tFG，这使得tFG分散体的利用非常有利(图5b)。
from graphite had concentrations much lower than those from
tFG, making the utilization of tFG dispersions highly
advantageous (Figure 5b). Second, the results here have not
其次，这里的结果还没有经过工业优化，如果逸出
的气体也能转化为石墨烯，那么使用压力电池可能会获得更好的结果。
been industrially optimized and would likely gain by using a
pressure cell have the escaping gases also convert to graphene.
此外，纳米tFG颗粒使tFG在少量表面活性剂存在下易于分散。
In addition, nanosized tFG particles make it easy to disperse
tFG的
tFG in the presence of a small amount of surfactant. The
质量以市场上可用的商用石墨烯的质量为基准。
quality of tFG was benchmarked against the quality of
commercial graphene available on the market. tFG was
发现tFG具有
明显更好的拉曼光谱，2D带更清晰，D带强度更低(图5c)。
found to have a significantly better Raman spectrum with a
sharper 2D band and lower D band intensity (Figure 5c). Also,
此外，
tFG的分散性远优于市售石墨烯，表明tFG在复合材料中的加工性能优于市售石墨烯。
tFG has dispersibility much better than that of commercial
graphene, indicating that tFG has better processability into
composites than commercial graphene. Given that the 98%
鉴于目前98%的石墨烯供应都是
低质量的石墨烯，46从PW商业规模生产tFG有可能提高市场上可用石墨烯的质量，并加速石
all graphene supplies are currently offering low-quality
墨烯相关技术从实验室向大规模工业的过渡。
graphene, producing tFG from PW on a commercial scale
could potentially elevate the quality of graphene available on
the market and accelerate the transition of graphene-related
technologies from laboratories to large-scale industries. To
为了证明tFG的有用性，测试了由HDPE衍生的tFG的硅酸盐水泥复合材料，发现从HDPE中添加
demonstrate the usefulness of tFG, Portland cement
0.035 wt%的FG可将硅酸盐水泥的抗压强度提高30%(图5d)。
composites of tFG derived from HDPE were tested to find
that adding 0.035 wt % of FG from HDPE increases the
compressive strength of Portland cement by 30% (Figure 5d).
这是由于通过添加tFG增加了水泥中硅酸钙水合物的完整性。
This is due to the increased integrity of calcium−silicate
使用石墨或碳纤维很难通过添
hydrates in cement *via* addition of tFG. Such enhancement
加少量tFG来提高抗压强度。
in the compressive strength by adding small fractions of tFG is
difficult to achieve with graphite or carbon fiber. For example,
例如，向水泥中添
加0.05 wt%的石墨，这几乎是我们复合材料中tFG负载的两倍，并没有导致抗压强度的显著
adding 0.05 wt % graphite to cement, which is almost double
变化。
the loading of tFG in our composites, did not result in a
noticeable change in the compressive strength. This shows
这表明tFG在大规
模应用中的优势，其中
the advantage of the tFG in large-scale applications where

https://dx.doi.org/10.1021/acsnano.0c06328
ACS Nano 2020, 14, 15595−15604

石墨烯负载量小意味着复合材料的物理性能显著增强。
small graphene loading translates into significant enhancement in the physical properties of composites.

收集AC-FJH过程中形成的蜡状物质，并通过傅立叶变换红外光谱(FTIR)进行分析，
The waxy substances formed during the AC-FJH process 发现蜡是具有FTIR指纹的低聚物，类似于氧化程度较低的母体塑料，如图6所示。
were collected and analyzed by Fourier transform infrared (FTIR) to find that the waxes are oligomers with FTIR fingerprints similar to the parent plastic with a low degree of oxidation, as shown in Figure 6. 捕蜡器设置示意图如图S28所示。A schematic of the wax trap 这些低聚物可以与石油烃流混合，加工成纯
setup is shown in Figure S28. These oligomers can be mixed 塑料，也可以用于生产洗涤剂复合材料的添加剂。
with petroleum hydrocarbon streams for processing into virgin plastic or can be used to produce additives for detergent 低聚物的产率小于10%，表明60%的闪蒸PW转化为气体产物。
composites. The yield of oligomers is <10%, indicating that ~60% of the flashed PW is transformed into gaseous product. 为了分析生成气体的成分，建立了一个闪蒸电极，电极表面钻有一个中心孔，旋转90°以
To analyze the composition of the generated gases, a flashing 允许挥发物逸出(图S29)。
electrode with a central hole drilled on the electrode face and a 90° turn to permit volatiles to escape was built (Figure S29). 在HDPE的FJH过程中释放的气体被捕获并收集在冷阱中。
The gases evolved during FJH of HDPE were captured and 根据196°C时挥发性流的蒸汽压计算出水成分
collected in a cold trap. An estimate of the effluent 的估计值；78°C(干冰浴)；23°C和60°C，表明该过程在
composition was calculated based on the vapor pressures of the volatile stream at −196 °C; −78 °C (dry ice bath); 23 and 60 °C, indicating that the process affords $H_2/C_{1-6}/C_{1-6}$ in a 5：4:1压力比(非摩尔比)。如果在结束后仍需生成类似量的H2
5:4:1 pressure ratio (not molar ratio). If a similar amount of H_2，则H2可用于燃料电池中，为FJH工艺生成清洁的补充电力。
remains to be generated upon scaling, then the H_2 might be used in a fuel cell to generate clean supplemental electricity for the FJH process.

CONCLUSIONS

使用少量电力将PW转化为高价值材料的能力使世界更接近塑料中性。
The ability to use small amounts of electricity to convert PW to higher value materials moves the world closer toward plastic 大规模使用FJH技术处理PW可能会减少从摇篮到升级周期使用塑料的温室气
neutrality. Using the FJH technology on a large scale to handle 体排放；然而，为了充分利用这种方法，还需要进行全生命周期分析。
PW could potentially reduce the emissions of greenhouse gases in cradle to upcycle use of plastics;[7,8,18] however, a full life-cycle analysis remains to be done for the full utility of this 据报道，生产1克纯PET需要38.8 kJ的能量，而使用FJH方法处理PW只需
approach. It has been reported that the production of 1 g of 要23 kJ，这是为了向上循环到tFG，而不仅仅是再循环。[49]
virgin PET requires 38.8 kJ of energy,[49] whereas treating PW using the FJH method will consume only 23 kJ, and this is for 众所周知，石墨
upcycling to tFG rather than merely recycling. Graphene is 烯是一种具有极强弹性结构的稳定碳源。
known to be a stable from of carbon with an extremely resilient 与石墨一样，石墨烯的微生物降解速度较慢，因此减少了重新进入碳循环。
structure. As with graphite, graphene can be slow in microbial degradation,[20,21] thereby lessening re-entry into the carbon 因此，应将PW的FJH视为对PW进行上循环的方法。
cycle. Therefore, FJH of PW should be considered as a method to upcycle PW.

METHODS

材料。CB(平均直径10 nm，黑珍珠2000)购自卡博特公司。
Materials. CB (average diameter 10 nm, Black Pearls 2000) was purchased from Cabot Corporation. 根据类型收集和分离可回收的PW。Recyclable PW was collected and 本研究报告的PW产品包括来自碳酸饮料瓶的PET、来自牛奶罐
separated based on type. The PW products reported in this work 或Polywize(德克萨斯州杰克逊维尔)的HDPE、来自水管的PVC、来自一次性塑料袋的LDPE、来自
include PET from carbonated beverage bottles, HDPE from milk jugs 一次性吸管和食品包装的PP以及来自一次性咖啡杯的PS。
or Polywize (Jacksonville, TX), PVC from plumbing pipes, LDPE from single use plastics bags, PP from disposable straws and food 使用上海科恒实业有限公司的
packaging, and PS from disposable coffee cups. The PW was sanded 切割机对粉末进行砂磨或切割，以获得粒径为1至2 mm的粉末。
or cut using a Shanghai Ke Heng Industrial Co. cutter to obtain 然后将粉末塑料与5 wt%炭黑混合以获得导电
powders with grain sizes 1 to 2 mm. The powdered plastic was then 混合物。可以用先前反
mixed with 5 wt % CB to obtain a conductive mixture. One could 应中制备的FG替代CB。在这里使用的某些情况下，
substitute CB with FG made in a prior reaction. In some cases used 粒径小于50 m的HDPE粉末作为原始材料从Millipore Sigma购买。
here, HDPE powder with grain size smaller the 50 μm was purchased as virgin material from Millipore-Sigma.

粉末填充在石英管中的两个铜电极之间(管厚度：2 mm，内径：8 mm，长度：5 cm)。
AC-FJH. Powders were packed between two copper electrodes in quartz tubes (tube thickness: 2 mm, inner diameter: 8 mm, length: 5 对样品进行压缩，以获得0.5 g塑料的120-125电阻率。
cm). The samples were compressed to obtain a resistivity of 120−125 在真空干燥器(10 mmHg)中对样品施加交流电(120 V，60 Hz)
Ω for 0.5 g of plastic. Alternating current (120 V, 60 Hz) was applied 8 s，以帮助放气。
to the sample for ~8 s in a vacuum desiccator (~10 mmHg) to aid 交流系统的详细说明见图S2。
with outgassing. A detailed description of the AC system can be found in Figure S2.

在AC-FJH后对样品进行DC-FJH。
DC-FJH. DC-FJH was performed on samples after AC-FJH. A 设计了一个由10个450 V和60 mF电容器组成的电容器组
capacitor bank composed of 10 capacitors of 450 V and 60 mF was 充电至110 V，并允许500 ms放电时间，以获得高质量FG。
charged to 110 V and allowed 500 ms discharge time to obtain high-quality FG. 直流电路的说明见图S1。The description of the DC circuit can be found in Figure S1.

表征 在50×物镜的Renishaw拉曼显微镜中，用532nm激光激发获得拉曼光谱。
Characterization. Raman spectra were obtained by excitation with a 532 nm laser in a Renishaw Raman microscope with a 50× 使用Rigaku D/Max Ultima II粉末XRD进行X射线衍射。
objective lens. X-ray diffraction was performed using a Rigaku D/Max 在TA仪器的Q50 TGA上进行TGA。
Ultima II powder XRD. TGA was performed on a Q50 TGA from TA 使用JEOL 2100F场发射枪TEM在200 kV下获得透射电子显微镜图像。
Instruments. Transmission electron microscopy images were acquired 使用
using JEOL 2100F field-emission gun TEM at 200 kV. X-ray PHI-Quantera SXM扫描X射线微探针在5×10 9托的基础压力下收集X射线光电子能谱。
photoelectron spectroscopy spectra were collected with a PHI Quantera SXM scanning X-ray microprobe with a base pressure of 使用0.5 eV步长记录测量光谱，通过能量为140 eV。
5×10^{-9} Torr. Survey spectra were recorded using 0.5 eV step sizes 使用0.1 eV步长记录元素光谱，通过能量为26 eV。
with a pass energy of 140 eV. Elemental spectra were recorded using 使用配备GoldenGate附件
0.1 eV step sizes with a pass energy of 26 eV. Fourier transform 的Thermo Scientific公司的Nicolet 6700 FTIR光谱仪收集傅立叶变换红外光谱。
infrared spectra were collected using a Nicolet 6700 FTIR spectrometer from Thermo-Scientific equipped with a GoldenGate accessory.

分散制剂。
Dispersion Preparations. FG solutions were prepared at 通过将FG悬浮在1 wt%Pluronic F-127溶液中并超
声30分钟以分散FG，制备浓度为1至10 g·L⁻¹的FG溶液。
concentrations from 1 to 10 g·L^{-1} by suspending FG in 1 wt % Pluronic F-127 solution and sonicating for 30 min to disperse FG. 超声处理后，在Beckman Coulter Allegra X-12离心机中以1500 rpm(470 rcf)的转速将分
After sonication, the dispersions were centrifuged in Beckman Coulter 散体离心30分钟，以去除骨料。
Allegra X-12 centrifuge equipped with a 19 cm in radius rotor at 1500 将上清液稀释500倍，并通过
rpm (470 rcf) for 30 min to remove aggregates. The supernatant was UV-vis(岛津UV-3600 plus)进行分析。
diluted 500 times and analyzed *via* UV−vis (Shimadzu UV-3600 在660 nm处记录吸光度，并使用660=6600 L·g 1·m 1的消光系数计算溶液中石墨烯的
plus). The absorbance was recorded at 660 nm, and an extinction 浓度。
coefficient of α_{660} = 6600 L·g^{-1}·m^{-1} was used to calculate the concentration of graphene in solution.

水泥复合材料制备。含1 wt%Pluronic F的FG-
Cement Composite Preparation. FG with 1 wt % Pluronic F-127在水中使用Silverson L5MA剪切混合器进行剪切混合
127 was shear mixed in water using a Silverson L5MA shear mixer for 以5000 rpm的速度运行15分钟，以形成暗色散。FG分
15 min at the speed of 5000 rpm to create a dark dispersion. FG 散体与硅酸盐水泥混合，分散比为0.40。接下来，将浆料浇铸在4.90×4.90×4.90 cm PTFE立方体
dispersions were mixed with Portland cement using a dispersion to 模具中(用于抗压强度)，并放置24小时。
cement ratio of 0.40. Next, the slurry was cast in 4.90 × 4.90 × 4.90 cm PTFE cube molds (for compressive strength) and were allowed to 7天后，使用带有双称重传感器的Forney变频驱动自动机器测量抗压强度。
set for 24 h. The compressive strength was measured after 7 days using a Forney variable frequency drive automatic machine with dual load cells.

ASSOCIATED CONTENT

Supporting Information

The Supporting Information is available free of charge at https://pubs.acs.org/doi/10.1021/acsnano.0c06328.

Schematic of AC-FJH equipment, Raman spectra, energy conversion calculations and other graphs and data (PDF)

AUTHOR INFORMATION

Corresponding Author

James M. Tour — *Department of Chemistry, Department of Materials Science and NanoEngineering, and Smalley-Curl Institute, NanoCarbon Center and Welch Institute for Advanced Materials, Rice University, Houston, Texas 77005, United States*; orcid.org/0000-0002-8479-9328; Email: tour@rice.edu

Authors

Wala A. Algozeeb — *Department of Chemistry, Rice University, Houston, Texas 77005, United States*

Paul E. Savas — *Department of Chemistry, Rice University, Houston, Texas 77005, United States*

Duy Xuan Luong — *Department of Chemistry, Rice University, Houston, Texas 77005, United States*; orcid.org/0000-0001-7089-3359

Weiyin Chen — *Department of Chemistry, Rice University, Houston, Texas 77005, United States*

https://dx.doi.org/10.1021/acsnano.0c06328
ACS Nano 2020, 14, 15595−15604

Carter Kittrell — *Department of Chemistry, Rice University, Houston, Texas 77005, United States;* orcid.org/0000-0002-8449-4292

Mahesh Bhat — *C-Crete Technologies, Stafford, Texas 77477, United States*

Rouzbeh Shahsavari — *C-Crete Technologies, Stafford, Texas 77477, United States*

Complete contact information is available at: https://pubs.acs.org/10.1021/acsnano.0c06328

Notes

The authors declare the following competing financial interest(s): Rice University owns intellectual property on the FG process which has been licensed to Universal Matter Ltd. JMT is a stockholder in Universal Matter Ltd. but not an officer or director. Conflicts of interest are managed by regular disclosure to the Rice University Office of Sponsored Programs and Research Compliance. C-Crete Technologies owns intellectual property on the strengthening of graphene-cement/concrete composites.

ACKNOWLEDGMENTS

We thank the Air Force Office of Scientific Research (FA9550-19-0296) and the Department of Energy (DE-F0031794) for their support. We thank Andrea Rodriguez of FCC Environmental Services (Houston, TX) for helpful advice on postconsumer plastics and Brad Wright of Polywize (Jacksonville, TX) for providing postconsumer HDPE. We also thank Saudi Aramco for the fellowship support for W.A.A. R.S. thanks the partial support of NSF-DMR 1709051.

REFERENCES

(1) Barnes, S. J. Understanding Plastics Pollution: The Role of Economic Development and Technological Research. *Environ. Pollut.* **2019**, *249*, 812−821.

(2) Sharma, S.; Chatterjee, S. Microplastic Pollution, a Threat to Marine Ecosystem and Human Health: A Short Review. *Environ. Sci. Pollut. Res.* **2017**, *24*, 21530−21547.

(3) Tetu, S. G.; Sarker, I.; Schrameyer, V.; Pickford, R.; Elbourne, L. D. H.; Moore, L. R.; Paulsen, I. T. Plastic Leachates Impair Growth and Oxygen Production in Prochlorococcus, the Ocean's Most Abundant Photosynthetic Bacteria. *Commun. Biol.* **2019**, *2*, 184−193.

(4) Lithner, D.; Nordensvan, I.; Dave, G. Comparative Acute Toxicity of Leachates from Plastic Products Made of Polypropylene, Polyethylene, PVC, Acrylonitrile−Butadiene−Styrene, and Epoxy to Daphnia Magna. *Environ. Sci. Pollut. Res.* **2012**, *19*, 1763−1772.

(5) Prata, J. C. Airborne Microplastics: Consequences to Human Health? *Environ. Pollut.* **2018**, *234*, 115−126.

(6) Cox, K. D.; Covernton, G. A.; Davies, H. L.; Dower, J. F.; Juanes, F.; Dudas, S. E. Human Consumption of Microplastics. *Environ. Sci. Technol.* **2019**, *53*, 7068−7074.

(7) Zheng, J.; Suh, S. Strategies to Reduce the Global Carbon Footprint of Plastics. *Nat. Clim. Change* **2019**, *9*, 374−378.

(8) Dormer, A.; Finn, D. P.; Ward, P.; Cullen, J. Carbon Footprint Analysis in Plastics Manufacturing. *J. Cleaner Prod.* **2013**, *51*, 133−141.

(9) Al-Salem, S. M.; Lettieri, P.; Baeyens, J. Recycling and Recovery Routes of Plastic Solid Waste (PSW): A Review. *Waste Manage.* **2009**, *29*, 2625−2643.

(10) Hopewell, J.; Dvorak, R.; Kosior, E. Plastics Recycling: Challenges and Opportunities. *Philos. Trans. R. Soc., B* **2009**, *364*, 2115−2126.

(11) Awasthi, A. K.; Shivashankar, M.; Majumder, S. Plastic Solid Waste Utilization Technologies: A Review. *IOP Conf. Ser.: Mater. Sci. Eng.* **2017**, *263*, No. 022024.

(12) Panda, A. K. Thermo-Catalytic Degradation of Different Plastics to Drop in Liquid Fuel Using Calcium Bentonite Catalyst. *Int. J. Ind. Chem.* **2018**, *9*, 167−176.

(13) Kumar, S.; Singh, R. K. Recovery of Hydrocarbon Liquid from Waste High Density Polyethylene by Thermal Pyrolysis. *Braz. J. Chem. Eng.* **2011**, *28*, 659−667.

(14) Kiran Ciliz, N.; Ekinci, E.; Snape, C. E. Pyrolysis of Virgin and Waste Polypropylene and its Mixtures with Waste Polyethylene and Polystyrene. *Waste Manage.* **2004**, *24*, 173−181.

(15) Budsaereechai, S.; Hunt, A. J.; Ngernyen, Y. Catalytic Pyrolysis of Plastic Waste for the Production of Liquid Fuels for Engines. *RSC Adv.* **2019**, *9*, 5844−5857.

(16) Eriksson, O.; Finnveden, G. Plastic Waste as a Fuel - CO_2-Neutral or Not? *Energy Environ. Sci.* **2009**, *2*, 907−914.

(17) Gibb, B. C. Plastics are Forever. *Nat. Chem.* **2019**, *11*, 394−395.

(18) Geyer, R.; Jambeck, J. R.; Law, K. L. Production, Use, and Fate of All Plastics Ever Made. *Sci. Adv.* **2017**, *3*, No. e1700782.

(19) Luong, D. X.; Bets, K. V.; Algozeeb, W. A.; Stanford, M. G.; Kittrell, C.; Chen, W.; Salvatierra, R. V.; Ren, M.; McHugh, E. A.; Advincula, P. A.; Wang, Z.; Bhatt, M.; Guo, H.; Mancevski, V.; Shahsavari, R.; Yakobson, B. I.; Tour, J. M. Gram-Scale Bottom-Up Flash Graphene Synthesis. *Nature* **2020**, *577*, 647−651.

(20) Krishnamurthy, A.; Gadhamshetty, V.; Mukherjee, R.; Chen, Z.; Ren, W.; Cheng, H. M.; Koratkar, N. Passivation of Microbial Corrosion Using a Graphene Coating. *Carbon* **2013**, *56*, 45−49.

(21) Hsieh, Y. P.; Hofmann, M.; Chang, K. W.; Jhu, J. G.; Li, Y. Y.; Chen, K. Y.; Yang, C. C.; Chang, W. S.; Chen, L. C. Complete Corrosion Inhibition through Graphene Defect Passivation. *ACS Nano* **2014**, *8*, 443−448.

(22) Novoselov, K. S.; Fal'ko, V. I.; Colombo, L.; Gellert, P. R.; Schwab, M. G.; Kim, K. A Roadmap for Graphene. *Nature* **2012**, *490*, 192−200.

(23) Nan, H. Y.; Ni, Z. H.; Wang, J.; Zafar, Z.; Shi, Z. X.; Wang, Y. Y. The Thermal Stability of Graphene in Air Investigated by Raman Spectroscopy. *J. Raman Spectrosc.* **2013**, *44*, 1018−1021.

(24) Li, Y.; Feng, L.; Shi, X.; Wang, X.; Yang, Y.; Yang, K.; Liu, T.; Yang, G.; Liu, Z. Surface Coating-Dependent Cytotoxicity and Degradation of Graphene Derivatives: Towards the Design of Non-Toxic. *Small* **2014**, *10*, 1544−1554.

(25) d'Amora, M.; Lamberti, A.; Fontana, M.; Giordani, S. Toxicity Assessment of Laser-Induced Graphene by Zebrafish During Development. *J. Phys. Mater.* **2020**, *3*, No. 034008.

(26) Ferrari, A. C. Raman Spectroscopy of Graphene and Graphite: Disorder, Electron−Phonon Coupling, Doping and Nonadiabatic Effects. *Solid State Commun.* **2007**, *143*, 47−57.

(27) Cançado, L. G.; Takai, K.; Enoki, T.; Endo, M.; Kim, Y. A.; Mizusaki, H.; Jorio, A.; Coelho, L. N.; Magalhães-Paniago, R.; Pimenta, M. A. General Equation for the Determination of the Crystallite Size L_a of Nanographite by Raman Spectroscopy. *Appl. Phys. Lett.* **2006**, *88*, 163106.

(28) Pimenta, M. A.; Dresselhaus, G.; Dresselhaus, M. S.; Cançado, L. G.; Jorio, A.; Saito, R. Studying Disorder in Graphite-Based Systems by Raman Spectroscopy. *Phys. Chem. Chem. Phys.* **2007**, *9*, 1276−1290.

(29) Schmucker, S. W.; Cress, C. D.; Culbertson, J. C.; Beeman, J. W.; Dubon, O. D.; Robinson, J. T. Raman Signature of Defected Twisted Bilayer Graphene. *Carbon* **2015**, *93*, 250−257.

(30) You, Y.; Ni, Z.; Yu, T.; Shen, Z. Edge Chirality Determination of Graphene by Raman Spectroscopy. *Appl. Phys. Lett.* **2008**, *93*, 163112.

(31) Kim, K.; Coh, S.; Tan, L. Z.; Regan, W.; Yuk, J. M.; Chatterjee, E.; Crommie, M. F.; Cohen, M. L.; Louie, S. G.; Zettl, A. Raman Spectroscopy Study of Rotated Double-Layer Graphene: Misorientation-Angle Dependence of Electronic Structure. *Phys. Rev. Lett.* **2012**, *108*, 246103.

(32) Garlow, J. A.; Barrett, L. K.; Wu, L.; Kisslinger, K.; Zhu, Y.; Pulecio, J. F. Large-Area Growth of Turbostratic Graphene on

Ni(111) *via* Physical Vapor Deposition. *Sci. Rep.* **2016**, *6*, 19804−19815.

(33) Niilisk, A.; Kozlova, J.; Alles, H.; Aarik, J.; Sammelselg, V. Raman Characterization of Stacking in Multi-Layer Graphene Grown on Ni. *Carbon* **2016**, *98*, 658−665.

(34) Hwang, J. S.; Lin, Y. H.; Hwang, J. Y.; Chang, R.; Chattopadhyay, S.; Chen, C. J.; Chen, P.; Chiang, H. P.; Tsai, T. R.; Chen, L. C.; Chen, K. H. Imaging Layer Number and Stacking Order Through Formulating Raman Fingerprints Obtained From Hexagonal Single Crystals of Few Layer Graphene. *Nanotechnology* **2013**, *24*, No. 015702.

(35) Stanford, M. G.; Bets, K. V.; Luong, D. X.; Advincula, P. A.; Chen, W.; Li, J. T.; Wang, Z.; McHugh, E. A.; Algozeeb, W. A.; Yakobson, B. I.; Tour, J. M. Flash Graphene Morphologies. *ACS Nano* **2020**, DOI: 10.1021/acsnano.0c05900.

(36) Vodakov, Y. A.; Mokhov, E. N.; Ramm, M. G.; Roenkov, A. D. Epitaxial Growth of Silicon Carbide Layers by Sublimation Sandwich Method (I) Growth Kinetics in Vacuum. *Krist. Tech.* **1979**, *14*, 729−740.

(37) Abrahamson, J. Graphite Sublimation Temperatures, Carbon Arcs and Crystallite Erosion. *Carbon* **1974**, *12*, 111−141.

(38) Majdzadeh-Ardakani, K.; Zekriardehani, S.; Coleman, M. R.; Jabarin, S. A. A Novel Approach to Improve the Barrier Properties of PET/Clay Nanocomposites. *Int. J. Polym. Sci.* **2017**, *2017*, 7625906.

(39) Lin, J.; Peng, Z.; Liu, Y.; Ruiz-Zepeda, F.; Ye, R.; Samuel, E. L. G.; Yacaman, M. J.; Yakobson, B. I.; Tour, J. M. Laser-Induced Porous Graphene Films from Commercial Polymers. *Nat. Commun.* **2014**, *5*, 5714.

(40) Li, Z. Q.; Lu, C. J.; Xia, Z. P.; Zhou, Y.; Luo, Z. X-ray Diffraction Patterns of Graphite and Turbostratic Carbon. *Carbon* **2007**, *45*, 1686−1695.

(41) Warren, B. E. X-Ray Diffraction in Random Layer Lattices. *Phys. Rev.* **1941**, *59*, 693−698.

(42) Lotya, M.; King, P. J.; Khan, U.; De, S.; Coleman, J. N. High-Concentration, Surfactant-Stabilized Graphene Dispersions. *ACS Nano* **2010**, *4*, 3155−3162.

(43) Seo, J.-W. T.; Green, A. A.; Antaris, A. L.; Hersam, M. C. High-Concentration Aqueous Dispersions of Graphene Using Nonionic, Biocompatible Block Copolymers. *J. Phys. Chem. Lett.* **2011**, *2*, 1004−1008.

(44) Johnson, D. W.; Dobson, B. P.; Coleman, K. S. A Manufacturing Perspective on Graphene Dispersions. *Curr. Opin. Colloid Interface Sci.* **2015**, *20*, 367−382.

(45) Hernandez, Y.; Nicolosi, V.; Lotya, M.; Blighe, F. M.; Sun, Z.; De, S.; McGovern, I. T.; Holland, B.; Byrne, M.; Gun'Ko, Y. K.; Boland, J. J.; Niraj, P.; Duesberg, G.; Krishnamurthy, S.; Goodhue, R.; Hutchison, J.; Scardaci, V.; Ferrari, A. C.; Coleman, J. N. High-Yield Production of Graphene by Liquid-Phase Exfoliation of Graphite. *Nat. Nanotechnol.* **2008**, *3*, 563−568.

(46) Kauling, A. P.; Seefeldt, A. T.; Pisoni, D. P.; Pradeep, R. C.; Bentini, R.; Oliveira, R. V. B.; Novoselov, K. S.; Castro Neto, A. H. The Worldwide Graphene Flake Production. *Adv. Mater.* **2018**, *30*, 1803784.

(47) Meng, W.; Khayat, K. H. Mechanical Properties of Ultra-High-Performance Concrete Enhanced with Graphite Nanoplatelets and Carbon Nanofibers. *Composites, Part B* **2016**, *107*, 113−122.

(48) Shahsavari, R. Hierarchical Modeling of Structure and Mechanics of Cement Hydrate. Ph.D. Thesis, MIT, Cambridge, 2011.

(49) Perugini, F.; Mastellone, M. L.; Arena, U. A Life Cycle Assessment of Mechanical and Feedstock Recycling Options for Management of Plastic Packaging Wastes. *Environ. Prog.* **2005**, *24*, 137−154.

https://dx.doi.org/10.1021/acsnano.0c06328
ACS Nano 2020, 14, 15595−15604